Drawing Dispersion Curves: Band Structure Customization via Nonlocal Phononic Crystals

Arash Kazemi[1,*] Kshiteej J. Deshmukh[2,*] Fei Chen[1,*] Yunya Liu,[1] Bolei Deng,[3,4]
Henry Chien Fu[1,†] and Pai Wang[1,‡]

[1]*Department of Mechanical Engineering, University of Utah, Salt Lake City, Utah 84112, USA*
[2]*Department of Mathematics, University of Utah, Salt Lake City, Utah 84112, USA*
[3]*Department of Electrical Engineering and Computer Science, Massachusetts Institute of Technology, Cambridge, Massachusetts 02139, USA*
[4]*Department of Mechanical Engineering, Massachusetts Institute of Technology, Cambridge, Massachusetts 02139, USA*

Dispersion relations govern wave behaviors, and tailoring them is a grand challenge in wave manipulation. We demonstrate the inverse design of phononic dispersion using nonlocal interactions on one-dimensional spring-mass chains. For both single-band and double-band cases, we can achieve any valid dispersion curves with analytical precision. We further employ our method to design phononic crystals with multiple ordinary (roton or maxon) and higher-order (undulation) critical points and investigate their wave packet dynamics.

Phononic crystals and vibroelastic metamaterials are architected heterogeneous solids for the manipulation of mechanical waves. They can exhibit many unconventional properties, such as frequency band gaps [1–7], negative refraction [8–11], and topologically protected modes [12–15]. They also have a wide range of applications in cloaking [16–20], signal manipulation [21,22], focusing [23,24], and energy trapping [25–27]. Recently, by incorporating nonlocal (i.e., farther than nearest neighbor) interactions [28], Rosa and Ruzzene [29–32] demonstrated diffusive transport, and Wu and Huang [33,34] investigated active control, while Chen *et al.* [35] showed rotonlike dispersion [36–42], where the local minimum of the dispersion curve resembles the roton behavior [43–45] of the helium-4 superfluid [46–50] at low temperature. All these exotic and desirable dynamic behaviors hinge on the dispersion relation—how frequency depends on wave vector—that is intrinsic to each particular design. However, most studies so far have been focused on the forward problem from a given design to a set of band structures. It is a long-standing goal in the research community to solve the inverse problem from given dispersion bands to actual metamaterial designs so that exotic behaviors and functionalities can be realized on demand. Prior efforts to tailor specific dispersions [51–55] or band gaps [56–59] typically relied on iterative searches with high computational costs, and they had only very limited success.

In this Letter, we demonstrate a design methodology that uses nonlocal interactions to customize dispersion relations. First, we present an analytical protocol to solve the inverse problem, achieving any arbitrarily defined single-band dispersion on monoatomic nonlocal chains. Then, we use this design protocol to obtain dispersion curves with ordinary and higher-order critical points. Using time-domain simulations, we illustrate their unconventional wave dynamics, especially at the undulation point (also known as stationary inflection point), where both the first and second derivatives of the dispersion curve vanish. This results in highly concentrated vibration energy since the wave mode is simultaneously nonpropagating and nonspreading. Finally, we also investigate the diatomic nonlocal chain and develop the design protocol to customize its two dispersion bands.

We start with a one-dimensional "monoatomic" phonon chain of identical masses, m, and linear springs. A schematic of the model is depicted in Fig. 1(a). Each mass
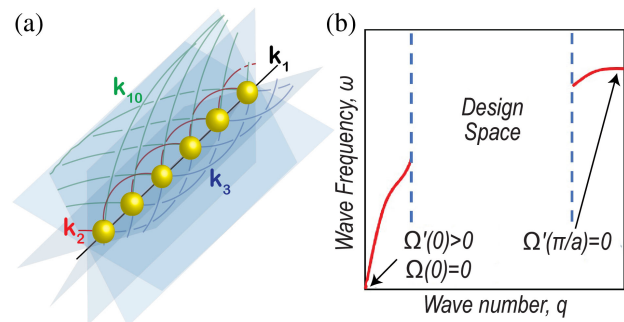

FIG. 1. (a) An infinite chain of identical masses. Each mass is connected to its nth-nearest neighbors with spring constant k_n. (b) The design space with fundamental constraints at the center ($q = 0$) and edge ($q = \pi/a$) of the first Brillouin zone.

is connected with its two nearest neighbors by local interactions with the spring constant k_1. In addition, each mass is also connected on both sides to its two nth-nearest neighbors with nonlocal interactions specified by the spring constants k_n, for $n = 2, 3, 4, …, N$, where N is the longest-range nonlocal interaction in the system. The governing equation of motion for the jth mass is

$$m\ddot{u}_j = \sum_{n=1}^{N} k_n(u_{j+n} - 2u_j + u_{j-n}). \qquad (1)$$

Based on the Bloch theorem [60], we obtain the following dispersion relation:

$$\omega^2(q) = \frac{2}{m}\left(\sum_{n=1}^{N} k_n - \sum_{n=1}^{N} k_n \cos(nqa)\right), \qquad (2)$$

where ω is the frequency, q is the wave number, and a is the spatial period of the lattice. For conventional chains with local springs k_1 only, Eq. (2) reduces to the classical result of $\omega^2(q) = (4k_1/m)\sin^2(qa/2)$, which is always monotonic and reaches its maximum at the Brillouin zone boundary [61]. The nonlocal interactions, on the other hand, may give rise to local minima and maxima at the interior of the Brillouin zone, as recently demonstrated by Chen *et al.* [35] and earlier by Farzbod and Leamy [62].

Since Eq. (2) takes the form of a Fourier series, we can use it to tailor the nonlocal interactions to achieve any desirable dispersion behavior. Mathematically, this originates from the fact that the dynamic matrix or Hamiltonian takes the form of a circulant matrix. Before the demonstration of customization procedures, it is necessary to understand all constraints in possible dispersion relations. Here, we consider the following physical and symmetry principles as fundamental assumptions of the designer nonlocal phononic crystals: (i) passive with no energy input or output, (ii) freestanding with no grounded springs, (iii) time-reversal symmetric with no gyroscopic effect, and (iv) stable with a finite static stiffness.

Combining the above, we arrive at the requirements that, for any target dispersion relation $\Omega(q)$ defined on the non-negative half of the first Brillouin zone $(q \in [0, \pi/a])$ to be valid, it needs to be a smooth curve with [See Fig. 1(b)]:

$$\Omega(0) = 0, \quad 0 < \Omega'(0) < +\infty, \quad \text{and} \quad \Omega'(\pi/a) = 0. \qquad (3)$$

Given an arbitrarily specified dispersion relation, $\Omega(q)$, satisfying Eqs. (3), we can design a nonlocal phononic crystal using the following protocol. First, we find the Fourier coefficients as

$$A_n = \frac{2a}{\pi}\int_0^{\pi/a} \Omega^2(q)\cos(nqa)dq, \quad n = 1, 2, …, N. \qquad (4)$$

Then, the design can be obtained by

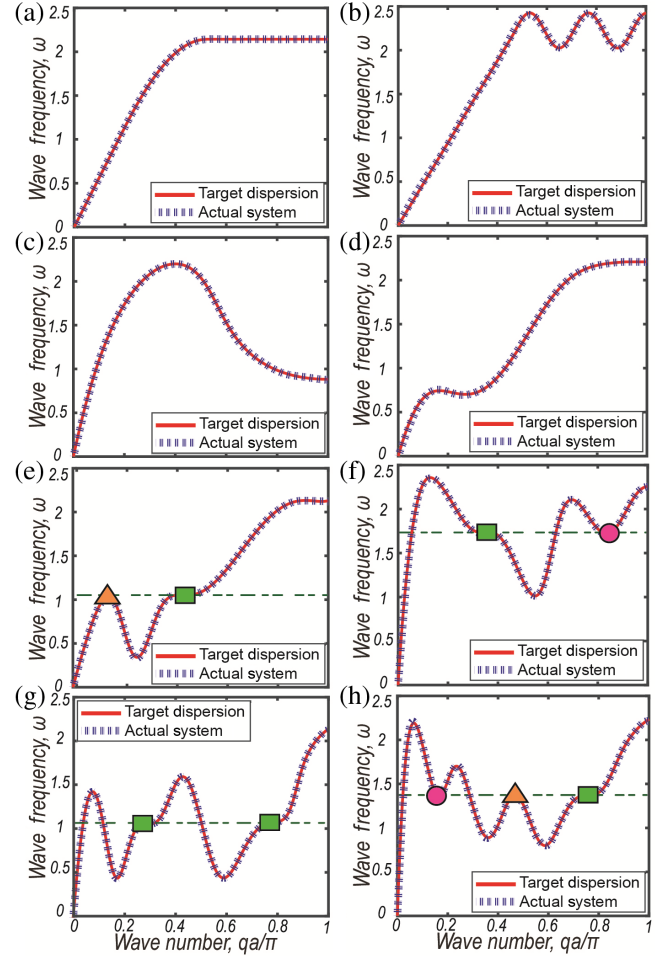
FIG. 2. Customized dispersion curves with special features.: (a) a flattop; (b)–(d) nonmonotonic behaviors at large, medium, and small wave number q (i.e., at short, medium, and long wavelength as compared to unit cell size), respectively; (e)–(h) undulation points (squares), maxons (triangles), and rotons (circles) occurring at the same frequency.

$$k_n/m = -A_n/2, \qquad n = 1, 2, …, N. \qquad (5)$$

Figure 2 shows results of this protocol with several examples. Since Eq. (5) shows all k_ns simply scale with m, we can set $m = 1$ for all cases. In each case, we compare the target dispersion with the actual one by examining the normalized root mean square deviation (NRMSD) between them. We purposefully choose the target curves with various interesting features. In the implementation, we use analytical functions as the targets for Figs. 2(a) and 2(b). For other cases, we use piecewise spline functions to construct target curves. The detailed procedures are given in the Supplemental Material [63]. For each target curve, the stiffness design variables are obtained using Eqs. (4) and (5). The total number of stiffness types is $N = 10$ for Figs. 2(a)–2(d), $N = 20$ for Figs. 2(e)–2(g), and $N = 25$ for Fig. 2(h), respectively.

The NRMSD is less than 1% in all cases, and the details are given in the Supplemental Materials [63]. We show that it is possible to achieve a flat band top [Fig. 2(a)] as well as nonmonotonic dispersion at relatively short [Fig. 2(b)], medium [Fig. 2(c)], and long [Fig. 2(d)] wavelength regimes. In addition, for critical points on the dispersion, we can design systems where local maxima (maxons), local minima (rotons), and stationary inflection points (undulations) can occur at the same frequency, as illustrated in Figs. 2(e) and 2(f).

Next, we investigate these critical points that exhibit exotic dynamics by considering two specific instances of nonlocal phononic crystals with the third-nearest-neighbor (k_3) interactions as the only nonlocal effect. When, $k_3 = 3k_1$ [Fig. 3(a), top], the dispersion curve is nonmonotonic [blue solid curve in Fig. 3(b)], exhibiting one local maximum (maxonlike) and one local minimum (rotonlike [35]) at $qa = 2\tan^{-1}(\sqrt{(11/7) \pm (6\sqrt{2}/7)})$. Both of them represent critical-point wave modes with zero group velocity (ZGV), and they are analogous to the Van Hove singularities [68] in electronic band structures. These ZGV modes also have promising applications in many wave-related engineering technologies such as noninvasive structural health monitoring [69–72] since the highly localized wave modes can enhance both the vibration energy concentration and the signal-to-noise ratio in ultrasonic probing. In contrast, when $k_3 = k_1/3$ [Fig. 3(a), bottom], the dispersion curve is monotonic [black dotted curve in Fig. 3(b)] with an undulation point in the middle at $qa = \pi/2$, where both the first and second derivatives vanish. While rotonlike dispersions were recently demonstrated [35–41], and undulation points of electromagnetic waves in optical waveguides were studied as frozen modes [73–75], we show here, for the first time, a second-order-critical undulation point for vibroelastic waves in phononic crystals.

To demonstrate wave behaviors at these critical points, we also perform two types of time-domain simulations on finite chains.

First, we apply a force excitation on the leftmost mass of a chain with 5000 unit cells. The forcing function is a Gaussian envelope in time:

$$f(t) = \exp\left[-(t-t_m)^2/\tau^2\right]\cos(\omega_c t), \tag{6}$$

where ω_c is the carrier frequency corresponding to the critical point, t_m is the peak time of the envelope, and $\tau = 100/\omega_c$ characterizes the time duration of the envelope. Figures 3(c) and 3(d) show the results for maxonlike and rotonlike dynamics, respectively, in the chain with $k_3 = 3k_1$. In each case, two modes of the same frequency but different wavelengths are observed: one is the traveling mode [hollow triangle and circle in [Fig. 3(b)] with finite group velocity, as indicated by the black dashed line, while the other is the ZGV mode [filled triangle and circle in
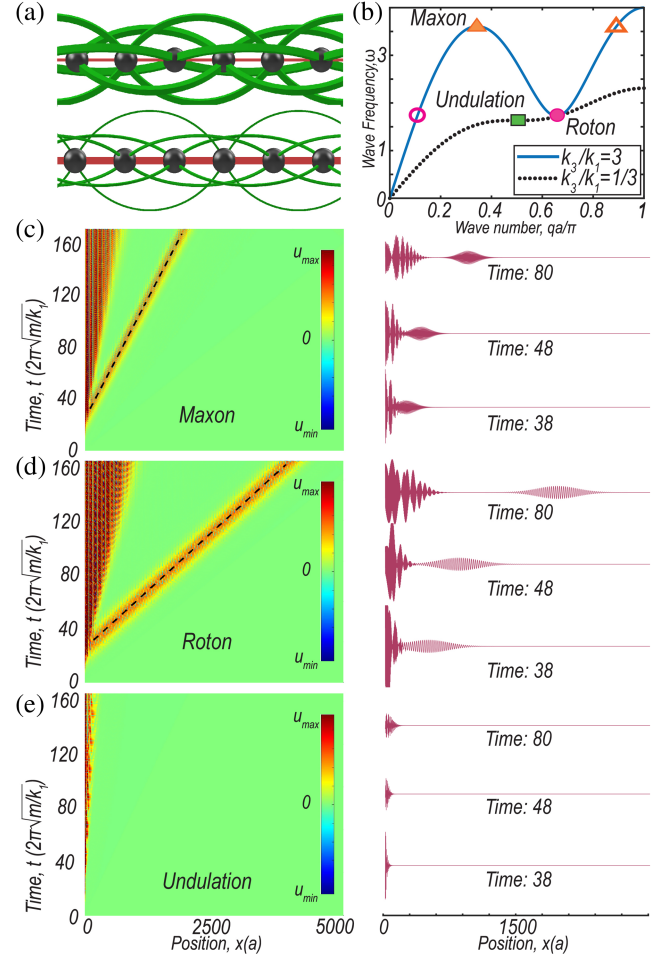

FIG. 3. (a) Schematics of two nonlocal phononic crystals with the first and third nearest-neighbor interactions only—top, $k_3 = 3k_1$; bottom, $k_3 = k_1/3$. (b) Dispersion curves. For $k_3 = 3k_1$, a local maximum (maxon) appears at $(\omega, qa/\pi) = (3.61, 0.344)$, and a local minimum (roton) appears at $(\omega, qa/\pi) = (1.72, 0.656)$. For $k_3 = k_1/3$, a stationary inflection point (undulation) appears at $(\omega, qa/\pi) = (1.63, 0.5)$, where both the first and second derivatives vanish. (c)–(e) Time-domain results for the 3 critical points in (b): maxon, roton, and undulation, respectively. The left column lists the time-space plots, while the right column shows wave amplitude snapshots.

Fig. 3(b)] localized at the source. Although the maxonlike and rotonlike ZGV modes are not traveling waves, the results show they do diffuse and spread out in space over time. In contrast, Fig. 3(e) shows the result at the undulation-point frequency on the chain with $k_3 = k_1/3$. Only one wave mode is observed. More importantly, not only is this mode nonpropagating, but it is also nonspreading, as both the group velocity, $\omega'(q)$, and the diffusion rate, $\omega''(q)$, vanish. This is a unique feature that does not exist in ordinary ZGV modes.

Second, to further investigate the diffusion phenomena, we look into the time evolution of a localized Gaussian spatial wave packet,
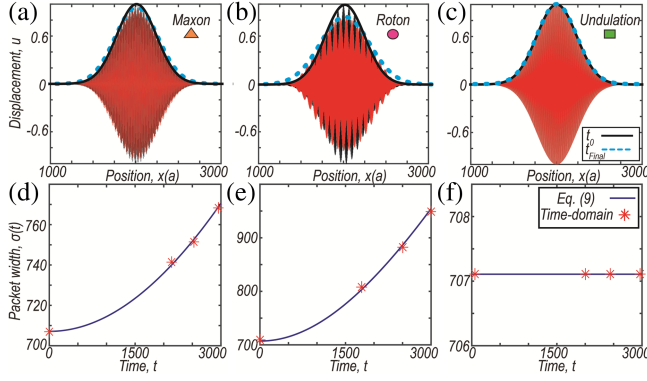
FIG. 4. Diffusion at the critical points. Evolution of an initially prescribed Gaussian packet with different carrier wave number q (i.e., different carrier wavelength) corresponding to the critical points in Fig. 3(b): (a) maxon mode with $qa/\pi = 0.656$, (b) roton mode with $qa/\pi = 0.344$, (c) undulation mode with $qa/\pi = 0.5$. The Gaussian envelope at time t_{Final} (blue dotted curve) is compared to the initial envelope at t_0 (black solid curve). (d)–(f) Theoretical and numerical values of $\sigma(t)$ vs t for each of the cases in (a)–(c), respectively, showing the spreading of wave envelopes.

$$u(x,t) = \exp\left[-(x-x_0)^2/\sigma(t)\right]\cos q_c x, \quad (7)$$

where q_c is the carrier wave number corresponding to the critical point, x_0 denotes the center of the wave packet, and $\sigma(t)$ characterizes the width of the envelope. We prescribe an initial Gaussian packet with $\sigma(t=0) = \sigma_0$. In each case, there is only one wave mode associated with the prescribed wave number q_c corresponding to the critical point, and it is a ZGV mode. As such, the wave packet does not propagate. However, the wave packet can still spread out or diffuse in space, i.e., while maintaining the same mean x_0, the envelope width $\sigma(t)$ changes, and its evolution over time is governed by [76]

$$\sigma(t) = \sigma_0\sqrt{1 + (t\omega''/\sigma_0^2)^2}. \quad (8)$$

Numerically, we can determine the diffusion rate of the wave packet by tracking $\sigma(t)$ in time-domain simulations on finite chains. Figures 4(a)–4(c) show the comparison of wave packet diffusion for the three critical points: local maximum (maxonlike), local minimum (rotonlike), and the undulation point (second order), respectively. In each case, the initial ($t=0$) wave envelope is represented by a black solid line. After evolving for sufficient time ($t = t_{Final}$) the resulting wave envelope is shown as a blue dotted line. Figures 4(d)–4(f) show, for each of the cases in Figs. 4(a)–4(c), respectively, the evolution of the packet width, $\sigma(t)$, at several time instances. Broadening of the envelope is observed for both maxon and roton packets, where $\omega' = 0$ but $\omega'' \neq 0$. In contrast, the wave envelope preserves its initial shape without diffusion in the case of the undulation point, where $\omega'' = \omega' = 0$. Lastly, we also

establish the customization protocol for the double-band system of a one-dimensional "diatomic" nonlocal phononic chain consisting of two different masses m_1 and m_2. This model leads to the following dispersion relations:

$$\omega_\pm^2 = K_0\left(\frac{1}{m_1} + \frac{1}{m_2}\right)$$
$$\mp \sqrt{K_0^2\left(\frac{1}{m_1} + \frac{1}{m_2}\right)^2 + \frac{1}{m_1 m_2}(K_1^2 - 4K_0^2)}, \quad (9)$$

where $-$ and $+$ in the $\mp$ sign denote the first and second bands (historically referred to as "acoustic" and "optical" branches), respectively. Here, K_0 and K_1 are

$$K_0(q) = \sum_{n=1}^{N} k_n - \sum_{\substack{n=2 \\ n\,\text{even}}}^{N} k_n \cos(nqa),$$

$$K_1(q) = 2\sum_{\substack{n=1 \\ n\,\text{odd}}}^{N} k_n \cos(nqa), \quad (10)$$

which are defined on the non-negative half of the first Brillouin zone, $q \in [0, \pi/(2a)]$. Given two arbitrarily specified smooth curves as the targets, $\Omega_-(q)$ and $\Omega_+(q)$, satisfying all fundamental and symmetry requirements detailed in the Supplemental Material [63], we can design a nonlocal chain using the following protocol. First, we calculate

$$\alpha = m_2/m_1 = \Omega_+^2\left(\frac{\pi}{2a}\right)\Big/\Omega_-^2\left(\frac{\pi}{2a}\right),$$
$$A(q) = [\Omega_+^2(q) + \Omega_-^2(q)]/2,$$
$$D(q) = [\Omega_+^2(q) - \Omega_-^2(q)]/2. \quad (11)$$

Then, we can get

$$K_0(q) = \alpha A(q)/(\alpha + 1),$$
$$K_1^2(q) = 4K_0^2(q) - \alpha A^2(q) + \alpha D^2(q). \quad (12)$$

Lastly, we obtain the stiffness values as

$$k_n = \frac{2a}{\pi}\int_0^{\frac{\pi}{2a}} K_1 \cos(naq)dq, \qquad n = 1, 3, 5, \ldots$$

$$k_n = -\frac{4a}{\pi}\int_0^{\frac{\pi}{2a}} K_0 \cos(naq)dq, \qquad n = 2, 4, 6, \ldots \quad (13)$$

We note that the above protocol is capable of customizing each individual band without affecting the other since it can work for two independently defined targets, $\Omega_-(q)$ and $\Omega_+(q)$. Figures 5(a)–5(d) show the results of this protocol by setting $m_1 = 1$. The target curves are purposefully chosen with various features: Fig. 5(a) demonstrates a rising first band with a flat second band; Fig. 5(b) shows
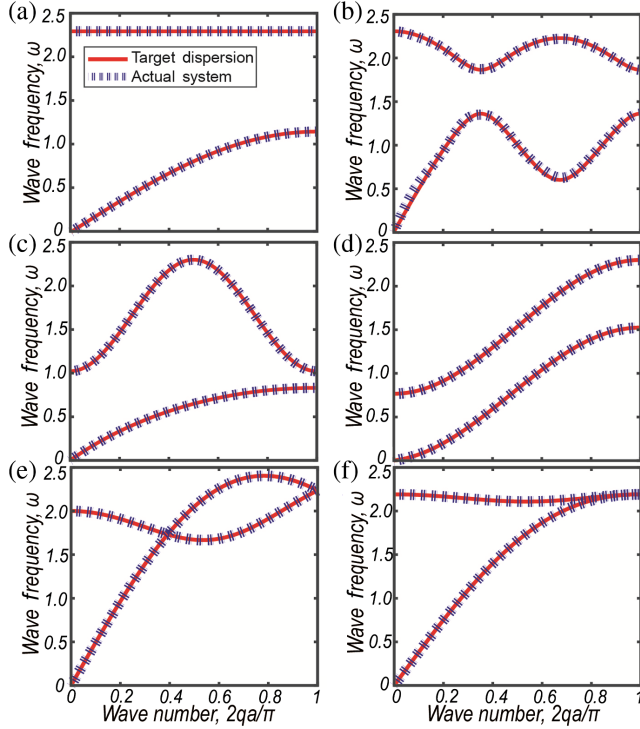
FIG. 5. (a)–(d) Customized double-band dispersion relations. black (e) and (f) show examples with linear (Dirac-like) and quadratic band crossings, respectively.

two bands with changing but always opposite convexity; Fig. 5(c) has a constant-curvature first band and an arched second band; and Fig. 5(d) has both bands monotonically increasing. These examples show that both localized and traveling wave modes can be designed at any arbitrarily desirable frequency and wavelength by our protocol on either band. In the implementation, we set the total number of stiffness types as $N = 20$ for Fig. 5. We also examine NRMSD values between the target and actual dispersion curves. The results show that, in most cases, a good match can be achieved with just a small number of nonlocal springs. Furthermore, we also demonstrate the protocol's capability of realizing linear (Dirac-cone-like) and quadratic band crossings in Figs. 5(e) and 5(f), respectively. Detailed information and additional examples are presented in the Supplemental Material [63].

In conclusion, we can completely and analytically customize the dispersion relations in phononic crystals by incorporating nonlocal springs. We show dispersion curves with multiple critical points of the first (maxon and roton) and second order (undulation). We further study the wave packet dynamics at each of the critical points and illustrate how we can use them to create novel behaviors of localized modes. This enables future research on higher-order critical points of elastic waves in terms of topology, scaling, and symmetry [77,78] in 2D and 3D systems. Finally, we can also solve the inverse problem for arbitrary two-band dispersion relations.

For practical considerations, physical samples of phononic metamaterials with a small number of nonlocal springs can be fabricated in relatively simple designs [38,41,79]. In fact, one-dimensional chains with any number of nonlocal connections are, at least in principle, feasible by the following reasoning: There are infinitely many planes that contain the line of masses. Hence, each nonlocal interaction can exist in a separate plane without interfering with others, similar to the design illustrations shown in Figs. 1(a) and 3(a), and in more detail in the Supplemental Material [63]. During the review process, we became aware of recent experimental efforts demonstrating nonlocal effects [80–83]. They provide further evidence supporting feasibility in design and fabrication. We are confident that future research efforts will enable more sophisticated experimental setups with many more nonlocal interactions in 2D and 3D phononic crystals and vibroelastic metamaterials.

At the continuum limit of the lattice constant $a \to 0$, wave mechanics in nonlocal continuum media can be described by higher-order strain-gradient models [84–86] as well as *peridynamics* [87,88]. In contrast to those popular phenomenological and semiphenomenological approaches, our method has the advantage of prescribing system parameters to achieve desirable dynamic behaviors. Homogenizing our design methodology could potentially provide a route to design the micromodulus elasticity kernel for target dispersion relations in continuum vibroelastic metamaterials.

[*]These authors contributed equally to this work.
[†]Corresponding author: henry.fu@utah.edu
[‡]Corresponding author: pai.wang@utah.edu

[1] Z. Liu, X. Zhang, Y. Mao, Y. Zhu, Z. Yang, C. T. Chan, and P. Sheng, Science **289,** 1734 (2000).
[2] P. Wang, F. Casadei, S. H. Kang, and K. Bertoldi, Phys. Rev. B **91,** 020103(R) (2015).
[3] S. G. Konarski, C. J. Naify, and C. A. Rohde, Appl. Phys. Lett. **116,** 051903 (2020).
[4] C. L. Willey, V. W. Chen, D. Roca, A. Kianfar, M. I. Hussein, and A. T. Juhl, Phys. Rev. Appl. **18,** 014035 (2022).
[5] I. Arretche and K. H. Matlack, J. Sound Vib. **540,** 117305 (2022).

[6] C. Widstrand, N. Kalantar, and S. Gonella, Extreme Mech. Lett. **53,** 101693 (2022).

[7] W. Ding, T. Chen, C. Chen, D. Chronopoulos, J. Zhu, and B. Assouar, Mech. Syst. Signal Process. **186,** 109922 (2023).

[8] N. Kaina, F. Lemoult, M. Fink, and G. Lerosey, Nature (London) **525,** 77 (2015).

[9] L. Fang and M. J. Leamy, *International Design Engineering Technical Conferences and Computers and Information in Engineering Conference* (American Society of Mechanical Engineers, 2021), 10.1115/DETC2021-71840.

[10] H. Danawe and S. Tol, J. Sound Vib. **518,** 116552 (2022).

[11] L. Fang and M. Leamy, J. Acoust. Soc. Am. **151,** A39 (2022).

[12] P. Wang, L. Lu, and K. Bertoldi, Phys. Rev. Lett. **115,** 104302 (2015).

[13] H. Danawe, H. Li, K. Sun, and S. Tol, Phys. Rev. Lett. **129,** 204302 (2022).

[14] K. Ding, C. Fang, and G. Ma, Nat. Rev. Phys. **4,** 745 (2022).

[15] M. Charara, J. McInerney, K. Sun, X. Mao, and S. Gonella, Proc. Natl. Acad. Sci. U.S.A. **119,** e2208051119 (2022).

[16] S. A. Cummer and D. Schurig, New J. Phys. **9,** 45 (2007).

[17] H. Nassar, Y. Y. Chen, and G. L. Huang, Phys. Rev. Lett. **124,** 084301 (2020).

[18] X. Xu, C. Wang, W. Shou, Z. Du, Y. Chen, B. Li, W. Matusik, N. Hussein, and G. Huang, Phys. Rev. Lett. **124,** 114301 (2020).

[19] F. Martinez and M. Maldovan, Mater. Today Phys. **27,** 100819 (2022).

[20] C. Xu, K. Lyu, and Y. Wu, Europhys. Lett. **141,** 15002 (2022).

[21] P. Karki and J. Paulose, Phys. Rev. Appl. **15,** 034083 (2021).

[22] N. Kruss and J. Paulose, Phys. Rev. Appl. **17,** 024020 (2022).

[23] C. Xu, G. Okudan, H. Danawe, D. Ozevin, and S. Tol, *Nondestructive Characterization and Monitoring of Advanced Materials, Aerospace, Civil Infrastructure, and Transportation XVI* (SPIE, 2022), pp. 189–196, 10.1117/12.2612906.

[24] G. Okudan, C. Xu, H. Danawe, S. Tol, and D. Ozevin, *Improved Detection of Localized Damage in Pipe-Like Structures Using Gradient-Index Phononic Crystal Lens* (Springer International Publishing,, Cham, 2022), 10.1007/978-3-031-07322-9_30.

[25] J. M. De Ponti, A. Colombi, E. Riva, R. Ardito, F. Braghin, A. Corigliano, and R. V. Craster, Appl. Phys. Lett. **117,** 143902 (2020).

[26] M. Alshaqaq, C. Sugino, and A. Erturk, Phys. Rev. Appl. **17,** L021003 (2022).

[27] J. E. Pechac and M. J. Frazier, Appl. Phys. Lett. **122,** 211702 (2023).

[28] R. Fleury, Nat. Phys. **17,** 766 (2021).

[29] M. I. Rosa and M. Ruzzene, New J. Phys. **22,** 053004 (2020).

[30] M. Nora Rosa and M. Ruzzene, F25.00013: Dynamics and Topology of Non-Hermitian Elastic Lattices with Non-Local Feedback Interactions (2020), https://meetings.aps.org/Meeting/MAR20/Session/F25.13.

[31] M. I. Rosa and M. Ruzzene, New J. Phys. **24,** 073020 (2022).

[32] M. I. N. Rosa and M. Ruzzene, *Proc. SPIE PC12048, Health Monitoring of Structural and Biological Systems XVI* (2022).

[33] Q. Wu and G. Huang, ASME Int. Mech. Eng. Congr. Expo. **85543,** V001T01A015 (2021).

[34] Q. Wu, P. Shivashankar, X. Xu, Y. Chen, and G. Huang, J. Compos. Mater. **57,** 771 (2023).

[35] Y. Chen, M. Kadic, and M. Wegener, Nat. Commun. **12,** 3278 (2021).

[36] C. Prada, D. Clorennec, and D. Royer, J. Acoust. Soc. Am. **124,** 203 (2008).

[37] H. Godfrin, M. Meschke, H.-J. Lauter, A. Sultan, H. M. Böhm, E. Krotscheck, and M. Panholzer, Nature (London) **483,** 576 (2012).

[38] J. A. Iglesias Martínez, M. F. Groß, Y. Chen, T. Frenzel, V. Laude, M. Kadic, and M. Wegener, Sci. Adv. **7,** eabm2189 (2021).

[39] J.-N. Schmidt, J. Hertkorn, M. Guo, F. Böttcher, M. Schmidt, K. S. H. Ng, S. D. Graham, T. Langen, M. Zwierlein, and T. Pfau, Phys. Rev. Lett. **126,** 193002 (2021).

[40] H. Lyu, Y. Zhang, and T. Busch, Phys. Rev. A **106,** 013302 (2022).

[41] K. Wang, Y. Chen, M. Kadic, C. Wang, and M. Wegener, Commun. Mater. **3,** 75 (2022).

[42] Y. Chen, M. A. Abouelatta, K. Wang, M. Kadic, and M. Wegener, Adv. Mater. **35,** 2209988 (2023).

[43] L. Landau, Phys. Rev. **60,** 356 (1941).

[44] E. B. Kolomeisky, J. Colen, and J. P. Straley, Phys. Rev. B **105,** 054509 (2022).

[45] L. Chomaz, R. M. van Bijnen, D. Petter, G. Faraoni, S. Baier, J. H. Becher, M. J. Mark, F. Waechtler, L. Santos, and F. Ferlaino, Nat. Phys. **14,** 442 (2018).

[46] R. P. Feynman, Phys. Rev. **94,** 262 (1954).

[47] D. Henshaw and A. Woods, Phys. Rev. **121,** 1266 (1961).

[48] M. S. Bryan and P. E. Sokol, Phys. Rev. B **97,** 184511 (2018).

[49] H. Godfrin, K. Beauvois, A. Sultan, E. Krotscheck, J. Dawidowski, B. Fåk, and J. Ollivier, Phys. Rev. B **103,** 104516 (2021).

[50] N. P. Müller and G. Krstulovic, Phys. Rev. B **105,** 014515 (2022).

[51] H. Goh and L. F. Kallivokas, J. Eng. Mech. **145,** 04019094 (2019).

[52] H.-W. Dong, C. Shen, S.-D. Zhao, W. Qiu, H. Zheng, C. Zhang, S. A. Cummer, Y.-S. Wang, D. Fang, and L. Cheng, Natl. Sci. Rev. **9,** nwac030 (2022).

[53] W. Jiang, Y. Zhu, G. Yin, H. Lu, L. Xie, and M. Yin, Mater. Today Phys. **22,** 100616 (2022).

[54] Z. Wang, J. Du, W. Shen, J. Liu, and Z. He, Sensors **21,** 6651 (2021).

[55] N. Arora, Q. Yao, and S. Rudykh, Extreme Mech. Lett. **51,** 101592 (2022).

[56] E. B. Isaacs and C. Wolverton, Chem. Mater. **30,** 1540 (2018).

[57] H. Goh and L. F. Kallivokas, Wave Motion **88,** 85 (2019).

[58] H. Goh and L. F. Kallivokas, Comput. Methods Appl. Mech. Eng. **370,** 113263 (2020).

[59] J. Morris, W. Wang, D. Shah, T. Plaisted, C. J. Hansen, and A. V. Amirkhizi, Mater. Des. **216,** 110510 (2022).

[60] M. I. Hussein, M. J. Leamy, and M. Ruzzene, Appl. Mech. Rev. **66,** 040802 (2014).

[61] A. S. Phani, Dyn. Lattice Mater. **1,** 53 (2017).

[62] F. Farzbod and M. J. Leamy, J. Vib. Acoust. **133,** 031010 (2011).

[63] See Supplemental Material at http://link.aps.org/supplemental/10.1103/PhysRevLett.131.176101 for additional results, detailed derivations, and calculation procedures, which includes Refs. [64–67].

[64] J. Mei, Y. Wu, C. T. Chan, and Z.-Q. Zhang, Phys. Rev. B **86,** 035141 (2012).

[65] A. Maznev, J. Acoust. Soc. Am. **135,** 577 (2014).

[66] M. Lanoy, F. Lemoult, A. Eddi, and C. Prada, Proc. Natl. Acad. Sci. U.S.A. **117,** 30186 (2020).

[67] C. Xu, G. Ma, Z.-G. Chen, J. Luo, J. Shi, Y. Lai, and Y. Wu, Phys. Rev. Lett. **124,** 074501 (2020).

[68] L. Van Hove, Phys. Rev. **89,** 1189 (1953).

[69] O. Balogun, T. W. Murray, and C. Prada, J. Appl. Phys. **102,** 064914 (2007).

[70] J. Laurent, D. Royer, T. Hussain, F. Ahmad, and C. Prada, J. Acoust. Soc. Am. **137,** 3325 (2015).

[71] A. Geslain, S. Raetz, M. Hiraiwa, M. Abi Ghanem, S. Wallen, A. Khanolkar, N. Boechler, J. Laurent, C. Prada, and A. Duclos, J. Appl. Phys. **120,** 135107 (2016).

[72] Y. Wu, R. Cui, K. Zhang, X. Zhu, and J. S. Popovics, NDT & E Int. **132,** 102727 (2022).

[73] H. Ramezani, S. Kalish, I. Vitebskiy, and T. Kottos, Phys. Rev. Lett. **112,** 043904 (2014).

[74] H. Li, I. Vitebskiy, and T. Kottos, Phys. Rev. B **96,** 180301(R) (2017).

[75] A. Herrero-Parareda, I. Vitebskiy, J. Scheuer, and F. Capolino, Adv. Photonics Res. **3,** 2100377 (2022).

[76] M. Remoissenet, *Waves Called Solitons: Concepts and Experiments* (Springer Berlin, Heidelberg, 2013), 10.1007/978-3-662-03790-4.

[77] N. F. Q. Yuan and L. Fu, Phys. Rev. B **101,** 125120 (2020).

[78] A. Chandrasekaran, A. Shtyk, J. J. Betouras, and C. Chamon, Phys. Rev. Res. **2,** 013355 (2020).

[79] Z. Zhu, Z. Gao, G.-G. Liu, Y. Ge, Y. Wang, X. Xi, B. Yan, F. Chen, P. P. Shum, H.-x. Sun *et al.,* New J. Phys. **24,** 123019 (2022).

[80] G. J. Chaplain, I. R. Hooper, A. P. Hibbins, and T. A. Starkey, Phys. Rev. Appl. **19,** 044061 (2023).

[81] D. B. Moore, J. R. Sambles, A. P. Hibbins, T. A. Starkey, and G. J. Chaplain, Phys. Rev. B **107,** 144110 (2023).

[82] A. Bossart and R. Fleury, Phys. Rev. Lett. **130,** 207201 (2023).

[83] A. R. Alisepahi, K. Sun, and J. Ma, arXiv:2304.04080.

[84] H. Askes, A. V. Metrikine, A. V. Pichugin, and T. Bennett, Philos. Mag. **88,** 3415 (2008).

[85] K. Deshmukh, T. Breitzman, and K. Dayal, J. Mech. Phys. Solids **167,** 104992 (2022).

[86] B. Wang, J. Liu, A. Soh, and N. Liang, Appl. Math. Mech. **43,** 1 (2022).

[87] S. A. Silling, J. Mech. Phys. Solids **48,** 175 (2000).

[88] S. A. Silling and R. B. Lehoucq, Adv. Appl. Mech. **44,** 73 (2010).